The final publication is available at

https://doi.org/10.1016/j.ultras.2018.03.011

Additional Information

Airborne non-contact and contact broadband ultrasounds for frequency attenuation profile estimation of cementitious materials

J. Gosálbez[a,*], W. M. D. Wright[b], W. Jiang[b], A. Carrión[a], V. Genovés[c], I.Bosch[a]

[a]*ITEAM, Universitat Politècnica de València, Camino de Vera, s/n 46022 Valencia, Spain*
[b] *Ultrasonic Research Group, University College Cork, College Road, Cork, Ireland*
[c]*ICITECH, Universitat Politècnica de València, Camino de Vera, s/n 46022 Valencia, Spain*

Abstract

In this paper, the study of frequency-dependent ultrasonic attenuation in strongly heterogeneous cementitious materials is addressed. To accurately determine the attenuation over a wide frequency range, it is necessary to have suitable excitation techniques. We have analysed two kinds of ultrasound techniques: contact ultrasound and airborne non-contact ultrasound. The mathematical formulation for frequency-dependent attenuation has been established and it has been revealed that each technique may achieve similar results but requires specific different calibration processes. In particular, the airborne non-contact technique suffers high attenuation due to energy losses at the air-material interfaces. Thus, its bandwidth is limited to low frequencies but it does not require physical contact between transducer and specimen. In contrast, the classical contact technique can manage higher frequencies but the measurement depends on the pressure between the transducer and the specimen.

Cement specimens have been tested with both techniques and frequency attenuation dependence has been estimated. Similar results were achieved at overlapping bandwidth and it has been demonstrated that the airborne non-contact ultrasound technique could be a viable alternative to the classical contact technique.

Keywords:
airborne ultrasound, attenuation, broadband signal, ultrasound, concrete, non-contact ultrasound

1. Introduction

Concrete is a non-homogeneous material that is composed of cement, aggregates and water, which is used mainly in the field of civil and building engineering [1]. Due to its non-homogeneous structure, in its hardened state this material may also include voids, unbonded interfaces between aggregates and cement paste, micro-cracks and other defects inside its micro structure. Consequently, its physical and mechanical properties are hard to quantify using nondestructive testing methods (NDT) [2]. Several authors have tried to test cement-based materials using different ultrasonic NDT techniques to characterise the properties of concrete and to monitor different damage parameters [3–5].

---

*Corresponding author E-mail adress: jorgocas@dcom.upv.es

Due to its robustness, ultrasonic pulse velocity is the most widely used ultrasonic parameter. However, its attenuation is considered more sensitive to the structural properties of the material. Given that it is an energy parameter, it is more easily affected by variability in the experimental setup than ultrasonic velocity, such as coupling problems between the ultrasonic sensor and the analysed material, energy loss due to cables, variability between sensors, and so on [6–9].

Despite these problems, the determination of the ultrasonic attenuation, and more specifically the frequency-dependent ultrasonic attenuation, $\alpha(f)$, [6, 8, 10–12], is useful because it is sensitive to different defects in materials (e.g. voids, cracks) and other properties, specifically in concrete where the water to cement ratio and cement to aggregate ratio are important variables in concrete design, and they determine its mechanical and physical properties.

Several different techniques have been used to measure the attenuation in cementitious materials. The most common setup is a contact through-transmission configuration, where the transmission transducer is excited with an electrical signal to generate the ultrasonic signal and the receiver transducer makes the reverse process. The inspected material is clamped between the transmitter and the receiver, and requires a coupling medium (usually water-gel, pure vaseline, or similar).

The transmitted signals can be narrowband ([8, 13–15]) or broadband ([6, 8, 16]). If the attenuation of the material and the sensitivity of measurement equipment allow the use of broadband signals, then the combination of this kind of measurement and suitable signal processing will result in an optimal estimate of $\alpha(f)$ with a minimum of measurement time [17]. Although these studies have focused on contact measures, some work has been carried out using airborne non-contact ultrasound or air-coupled ultrasound [18, 19]. This technique is quite similar to the contact technique but the transmitter and receiver are separated from the inspected material by an air gap of several centimetres. Therefore, the transducers are not in contact with the material and it does not require any liquid coupling. However, there are additional air-material interfaces that produce attenuation effects. Some studies combine broadband signals with time-frequency techniques to localize reinforcement bars in concrete [20], while others use airborne ultrasound to obtain velocity tomographies over cement probes [21].

The aim of this paper is to obtain the frequency-dependent attenuation, $\alpha(f)$, for cement-based specimens using air-coupled ultrasound and then compare it with the same attenuation obtained by means of normal contact ultrasound. For this work, a linear swept-frequency signal (chirp signal) will be used as a broadband signal in both cases because this kind of signal offers similar results to narrowband signals but with a lower temporal cost [17]. The rest of this manuscript is structured as follows. The first section contains the introduction, while mathematical models for attenuation measurements are described in the next section. Then, materials, ultrasonic layout and calibration process are presented in Section 3. The results and a discussion of the techniques, including a comparison, are presented in Section 4. Finally, the main conclusions are stated in Section 5.

2. Mathematical background

In a contact through-transmission inspection, the energy spectral density (ESD)[1] of the received signal (in the frequency domain), $S_{rx}(f)$ [dB], can be modelled as Eq. (1), where, $S_{tx}(f)$ [dB] is the ESD of the transmitted signal, α_{mat} [dB/cm] is the attenuation of the specimen, d_{mat} [cm] is the thickness of the specimen and $\alpha_{cal}(f)$ [dB] is the attenuation due to other factors (e.g. amplifiers, cables, frequency response of emitter and receiver transducers, etc).

$$S_{rx}(f) = S_{tx}(f) - \alpha_{mat}(f)d_{mat} - \alpha_{cal}(f) \tag{1}$$

Beginning with Eq. (1), the attenuation of the material, $\alpha_{mat}(f)$ [dB/cm], can be obtained as the difference between the transmitted signal, $S_{tx}(f)$ [dB] and the received signal, $S_{rx}(f)$ [dB] plus the calibration attenuation, $\alpha_{cal}(f)$ [dB], divided by the total thickness of the specimen, d_{mat} [cm], as shown in Eq. (2).

$$\alpha_{mat}(f) = \frac{S_{tx}(f) - S_{rx}(f) - \alpha_{cal}(f)}{d_{mat}} \tag{2}$$

The transmitted signal, $S_{tx}(f)$, conditions the frequencies that are injected into the analysed material and, therefore, the frequencies at which $\alpha_{mat}(f)$ can be evaluated. It is possible to use narrow band signals as a burst signal or a sinusoidal signal, or broadband signal as a chirp signal. The first ones have the advantage that most of the signal energy is concentrated over one frequency or a narrow bandwidth and the estimation of $\alpha_{mat}(f)$ will correspond only for that narrow bandwidth. On the other hand, broadband signals distribute the energy over a wider bandwidth and the estimation of $\alpha_{mat}(f)$ covers a higher bandwidth with one measurement, although with a lower signal to noise ratio than narrow bandwidth signals. This issue must be considered in highly dispersive media. Despite this, [17] demonstrated that broadband signals offer good accuracy with an important reduction of measurement time, therefore, chirp signals will be used in this study.

The $\alpha_{cal}(f)$ will also limit the bandwidth. This limitation is mainly due to the transducers and many authors often use transducers with different fundamental frequencies to characterize materials at different frequencies, but, as it was demonstrated in [17, 22], it is also possible to take advantage of their bandwidth and work outside of their fundamental frequency with good performance.

2.1. Attenuation model for contact measurements

For the contact method, the transducers directly touch the specimen (Fig. 1) and Eq. 2 may be re-written as Eq. 3, where the terms have been renamed with super-index (C). It must be noticed that $\alpha_{cal}(f)$ includes the effects of the measurement equipment: cables, amplifier and the frequency response of the emitter and receiver transducers plus the attenuation due to the boundaries transducer-specimen $(\alpha_{B_1}^{(C)})$ and specimen-material $(\alpha_{B_2}^{(C)})$.

---

[1]The energy spectral density, $S(f)$, of a finite time signal, $x(t)$, is defined as $S(f) = |X(f)|^2$, where $X(f) = \int_{t_0}^{t_1} x(t)e^{-\sqrt{-1}2\pi f t}dt$ is Fourier Transform of signal $x(t)$.

This means $\alpha_{cal}^{(C)}(f)$ is equal to $\alpha_{equip}^{(C)}(f)$ plus $\alpha_{B}^{(C)}(f)$, as shown in Eq. (4), where $\alpha_{B}^{(C)}(f) = \alpha_{B_1}^{(C)}(f) + \alpha_{B_2}^{(C)}(f)$. These terms must be estimated in order to obtain accurate results for material attenuation.
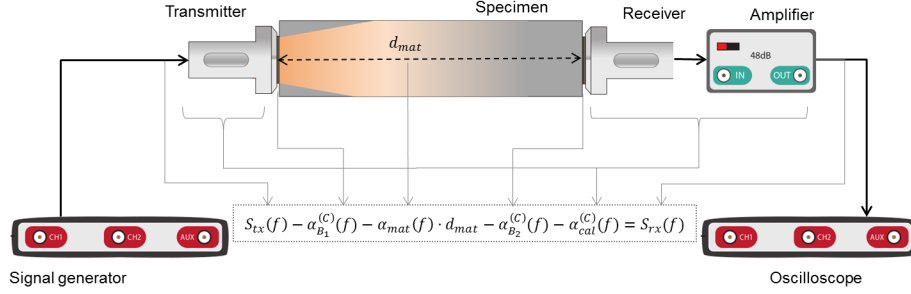

Figure 1: Layout of the equipment used in a contact inspection. The terms of Eq. 3 are identified in each stage of the scheme

$$\hat{\alpha}_{mat}^{(C)}(f) = \frac{S_{tx}(f) - S_{rx}(f) - \alpha_{cal}^{(C)}(f)}{d_{mat}} \tag{3}$$

$$\alpha_{cal}^{(C)}(f) = \alpha_{equip}^{(C)}(f) + \alpha_{B}^{(C)}(f) \tag{4}$$

2.2. Attenuation model for non-contact measurements

Eq. (1) and Eq. (2) are general expressions for ultrasonic contact through-transmission setups, but these expressions become more complex when non-contact ultrasound is used since additional attenuation terms must be added [23]. These additional terms are due to the propagation through the air and the additional air-material boundaries. Fig. 2 represents the attenuation model for the airborne non-contact method with additional attenuation terms, where $\alpha_{air}(f)(d_1 + d_2)$ [dB] represents the ultrasonic absorption in air which depends on the propagation distance, frequency, temperature and atmospheric pressure [24]. The terms $\alpha_{B_{in}}(f)$ [dB] and $\alpha_{B_{out}}(f)$ [dB] represent the attenuation due to reflection at the two air-material boundaries and depend on the acoustic impedance of both media [25]: the first term corresponds to the air-mortar boundary where the ultrasonic beam enters the material, and the second one corresponds to the mortar-air boundary where ultrasonic beam exits the material. The terms $\alpha_{S,in}(f, d_1)$ [dB] and $\alpha_{S,out}(f, d_2)$ [dB] represent the energy loss due to beam spread and depend on the specific emitter-receiver morphology, distance and frequency. The first term, $\alpha_{S,in}(f, d_1)$, corresponds to the spread of the ultrasonic beam when the transducer acts as the emitter and the mortar acts as receiver (transmission stage), meanwhile, the second one, $\alpha_{S,out}(f, d_2)$, corresponds to when the mortar acts as the emitter and the transducer acts as the receiver (reception stage) as shown in Fig. 2.

Then, Eq. (1) may be re-written as Eq. 5, where $\alpha_{cal}^{(NC)}(f)$ not only includes the attenuation due to the equipment but also the air propagation effects, as shown in Eq. (6). Finally, the material attenuation for non
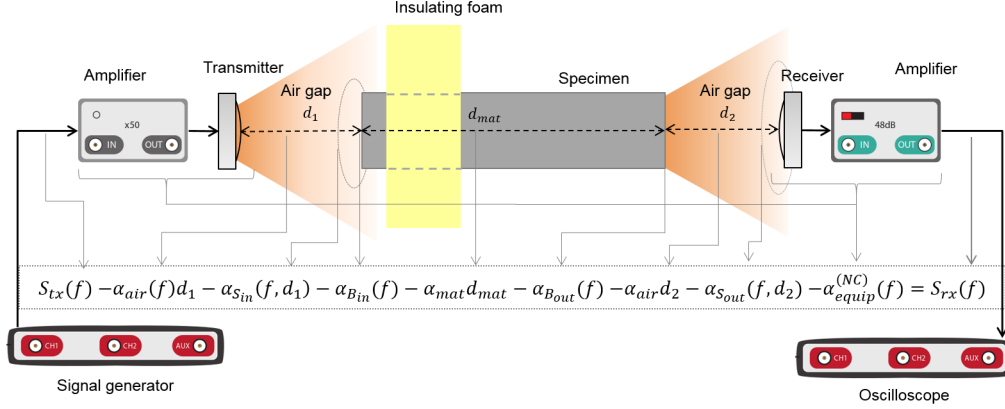
Figure 2: Layout of the equipment used in the non-contact ultrasonic inspection. The terms of Eq. (5) and Eq. (6) are identified in each stage of the scheme

contact measurements, $\hat{\alpha}_{mat}^{(NC)}$, is shown in Eq. (7). As previously commented for the contact method, $\alpha_{cal}^{(NC)}(f)$ must be estimated (Section 3.3.2).

$$S_{rx}(f) = S_{tx}(f) - \hat{\alpha}_{mat}^{(NC)}(f) - \alpha_{cal}^{(NC)}(f) \tag{5}$$

$$\alpha_{cal}^{(NC)}(f) = \alpha_{air}(f)d_1 + \alpha_{S_{in}}(f,d_1) + \alpha_{B_{in}}(f) + \alpha_{B_{out}}(f) + \alpha_{air}(f)d_2 + \alpha_{S_{out}}(f,d_2) + \alpha_{equip}^{(NC)}(f) \tag{6}$$

$$\hat{\alpha}_{mat}^{(NC)}(f) = \frac{S_{tx}(f) - S_{rx}(f) - \alpha_{cal}^{(NC)}(f)}{d_{mat}} \tag{7}$$

It is also noted that in the Fraunhofer region or far field, the maximum ultrasound pressure is found along the centreline of the transducer and the pressure distribution is more homogeneous than in the Fresnel region, but the beam is divergent. Meanwhile, in the Fresnel region or near field, the ultrasound pressure distribution is cylindrical but big pressure variations take place along the beam axis. Therefore, distances d_1 and d_2, that correspond to the transmission stage and reception stages respectively, were chosen to guarantee that both stages were carried out in the Fraunhofer zone (Section 3.2.2).

3. Experiment

3.1. Materials and sample preparation

Mortar specimens were manufactured according to Spanish standard UNE EN 196-1:2005 [26]. To improve the statistical analysis of the processed signals, three mixes were performed. Each mix is composed of 450 grams of CEM I 52,5-R cement, 1350 grams of silica sand and 225 grams of water. The result of these three mixes were nine specimens of 40x40x160 mm^3 standardized mortar, with 0.5 water to cement ratio and 1:3 cement to aggregate ratio. When the iron moulds were filled with the fresh mortar, they were first stored in a wet chamber

(20 °C and 100 % RH) for 24 hours. The specimens were then released and cured under water at 20 °C in the wet chamber for 90 days until the first test was performed. For this work, one specimen of each mix was chosen.

3.2. Test layout
3.2.1. Contact ultrasonic layout

An ultrasonic through-transmission setup was selected because it offers good penetration and good accuracy for attenuation estimation. The layout for the contact measurements is shown in Fig. 1. The transducers used were $K1SC$ (for transmission) and $K1SC$ (for reception), and they came from General Electric. They are both broadband transducers with a bandwidth greater than 70 % and centered at 1 MHz.

The transmitter transducer was directly excited by a programmable signal generator (Handyscope $HS3$) while the reception transducer was connected to a linear amplifier with a gain factor of 100 (EG&G Princeton 5113). The received and amplified ultrasonic signal was captured by a digital oscilloscope (Handyscope $HS3$) with a sampling frequency of 50 MHz. The number of acquired samples was 20000 samples, which corresponds to a temporal interval of 400 μs. Finally, a laptop was used to control the signal generator and to store the digitized signals from the oscilloscope.

The ultrasonic transducers were placed facing the longitudinal axis of the specimen, as shown in Fig. 1. They were fixed by two plastic clamps: a movable clamp that was used to adjust to the specimen, and a fixed clamp. Vaseline was used as an impedance coupling medium between the transducers and the specimen.

3.2.2. Non-contact ultrasonic layout

The layout of the air coupled measurements is shown in Fig. 2. The transducers that we used were Series 600 Environmental Grade Transducers from SensComp. Both were capacitive and broadband transducers, with a bandwidth centered at 50 kHz and an operating frequency ranging from 20 kHz up to 100 kHz. The transmitter transducer was excited by a programmable signal generator (Handyscope $HS3$) plus a linear amplifier with a gain factor of 50 (Falcosystem WMA-300) and a 200 V bias voltage. The reception transducer was connected to a charge amplifier($CA6/C$) from Cooknell Electronics, with a 100 V bias voltage plus a linear amplifier with a gain factor of 100 (EG&G Princeton 5113). The received and amplified ultrasonic signal was captured by a digital oscilloscope (Handyscope $HS3$), with a sampling frequency of 10 MHz. The number of acquired samples was 20000 samples, which corresponds to a temporal interval of 2 ms. Finally, a laptop was used to control the signal generator and to store the digitized signals from the oscilloscope, as previously. The transmitter and receiver transducers were separated by 16 cm each from the specimen and the perimeter of the specimen was covered by sound absorbing foam to block off ultrasonic signals that could propagate directly through the air between the transmitter and the receiver.

The SensComp transducer has a circular aperture size of 38.4 mm, and the near-field lengths for 10 kHz and 150 kHz signals were 1.1 cm and 16.1 cm, respectively, according to Eq. (8). Therefore, the separation between the emitter and the sample was established at 16 cm to guarantee operation in the far field region. Additionally,

the separation between the sample and the receiver (reception stage) was also fixed to 16 cm to guarantee a similar operation. It is demonstrated in Section 3.3.2 that the 40x40 mm mortar face has a similar ultrasonic beam pattern to the 38.4 mm Senscomp transducer.

$$d = \frac{D^2}{4\lambda} = \frac{D^2 f}{4c} \tag{8}$$

3.3. Calibration process

A calibration process is required to estimate the terms $\alpha_{cal}^{(C)}(f)$ and $\alpha_{cal}^{(NC)}(f)$, which include all of the attenuation effects external to the material: cables, connectors, transducers, amplifiers and propagation losses. Taking into account that two different methods were carried out with different technologies, two different calibration processes were required: contact calibration ($\alpha_{cal}^{(C)}(f)$) and non-contact calibration ($\alpha_{cal}^{(NC)}(f)$).

3.3.1. Contact calibration

The calibration process requires us to estimate $\alpha_{equip}^{(NC)}$ and $\alpha_B^{(C)}$. The first term, $\alpha_{equip}^{(NC)}$, was estimated with the emitter and receiver transducers face to face and no material between them. In this situation, and due to the absence of the material, Eq. (3) simplifies and it becomes Eq. (9),

$$S_{tx}(f) - S_{rx}(f) = \alpha_{equip}^{(C)} \tag{9}$$

where $S_{tx}(f)$ [dB] is the energy spectral density (ESD) of the transmitted signal and $S_{rx}(f)$ [dB] is the ESD of the received signal obtained during the calibration process. In this case, it is important to notice that $\alpha_{cal}^{(C)}(f)$ is equal to $\alpha_{equip}^{(C)}$ and no additional effects have to be taken into account. Fig. 3 shows the $-\alpha_{cal}^{(C)}(f)$ obtained from this calibration process. The parameters that we used during this process were identical to the material analysis parameters, except for the transmitted signal amplitude, which was reduced to 0.5 Vp to avoid saturation.

The second term, $\alpha_B^{(C)}(f)$, was estimated by means of the difference of two measurements taken on the same specimen but with different distances. The chosen probe was Probe C and it was measured at $d_1 = 16$ cm and at $d_2 = 10$ cm (the probe was cut for this second measure). Applying Eq. (3), two attenuations were obtained: $\hat{\alpha}_{d_1}^{(C)}(f)$ and $\alpha_{d_2}^{(C)}(f)$, respectively. As $\alpha_B^{(C)}(f)$ is not compensated yet, these attenuations have a bias due to $\alpha_B^{(C)}(f)$ (Eq. (10)). The difference between $\hat{\alpha}_{d_1}^{(C)}(f)$ and $\alpha_{d_2}^{(C)}(f)$ provides the term $\alpha_B^{(C)}(f)$, as shown in Eq. (11). This term has been assumed to not be frequency dependent because of the employed wavelength and its estimated value was 4.5 dB.

$$\hat{\alpha}_{d_i}^{(C)}(f) = \frac{S_{tx}(f) - S_{rx,d_i}(f) - \overbrace{\left(\alpha_{equip}^{(C)}(f) + \alpha_B^{(C)}(f) \right)}^{\alpha_{cal}^{(C)}(f)}}{d_i} = \hat{\alpha}_{mat}(f) - \frac{\alpha_B^{(C)}(f)}{d_i} \tag{10}$$

$$\alpha_B^{(C)}(f) = \frac{(\alpha_{d_1}^{(C)}(f) - \alpha_{d_2}^{(C)}(f)) d_1 d_2}{d_2 - d_1} \tag{11}$$
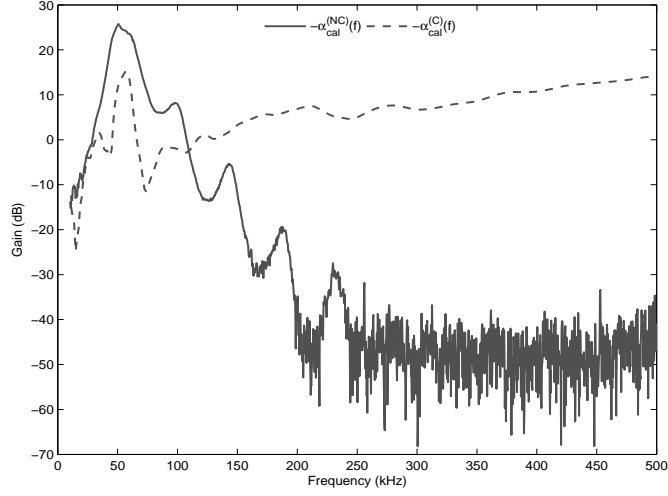
7

Figure 3: Gain frequency response of calibration process for non-contact and contact methods)

3.3.2. Non-contact calibration

For the non-contact method, the calibration process requires us to estimate more terms than the contact method due to propagation of ultrasound through air. As has been described in Eq. (6), $\alpha_{cal}^{(NC)}(f)$ is composed of several different terms: equipment attenuation ($\alpha_{equip}^{(NC)}(f)$), ultrasonic air attenuation ($\alpha_{air}(f)(d_1 + d_2)$), spread beam attenuation ($\alpha_{S,in}(f, d_1)$ and $\alpha_{S,out}(f, d_1)$), and boundary attenuations ($\alpha_{B_{in}}(f)$ and $\alpha_{B_{out}}(f)$).

To reach this aim, the calibration process was carried out with the emitter and receiver transducers face to face with $d_{cal} = d_1 + d_2 = 32$ cm separation and without any material between them (Fig. 4). In this situation, some terms from the original expresion Eq. (7) disappear due to the absence of the material, as shown in Eq. (12).
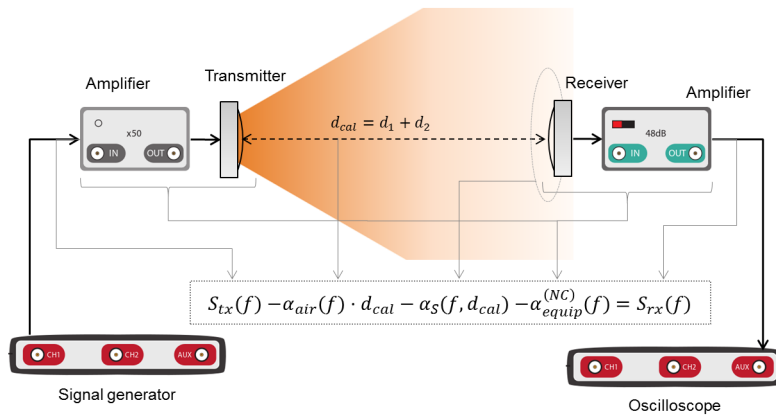

Figure 4: Calibration setup for non-contact equipments

8

$$S_{rx}(f) = S_{tx}(f) - \widetilde{\alpha_{mat}^{(NC)}(f)d_{mat}} - \overbrace{\left(\alpha_{air}(f)d_{cal} + \widetilde{\alpha_{B_{in}}(f)} + \widetilde{\alpha_{B_{out}}(f)} + \alpha_{equip}^{(NC)}(f) \right)}^{\alpha_{cal,1}^{(NC)}(f)} + \alpha_{S_{cal}}(f, d_{cal}) \qquad (12)$$

The difference between $S_{tx}(f)$ and $S_{rx}(f)$ offers us the first term for calibration process $\alpha_{cal,1}^{(NC)}(f)$, Eq. (13), which includes the attenuation due to the measurement equipment, $\alpha_{equip}^{(NC)}(f)$, the attenuation due to the air absorption $\alpha_{air}(f)d_{cal}$ and the attenuation due to beam spread $\alpha_{S_{cal}}(f, d_{cal})$.

$$\alpha_{cal,1}^{(NC)}(f) = S_{tx}(f) - S_{rx}(f) = \alpha_{equip}^{(NC)}(f) + \alpha_{air}(f)d_{cal} + \alpha_S(f, d_{cal}) \qquad (13)$$

The terms $\alpha_{equip}^{(NC)}(f)$ and $\alpha_{air}(f)d_{cal}$ that are obtained from this calibration process are similar to those that appear in the normal measurement process (d_{cal} has been fixed equal to $d_1 + d_2 = 32cm$), but not $\alpha_{S_{cal}}(f, d_{cal})$. This last term depends on the morphology and active surface of the emitter and it may be approximated by Eq. (14) [23], where d is is the transducer separation and θ_f (Eq. (15)) is the beam spread angle for f, which depends on the aperture of the ultrasonic transducer, D, and the wavelength, $\lambda = c/f$, in the medium through which the sound is travelling.

$$\alpha_S(f, d) = 20log_{10}\left(\frac{2d}{D}\tan\left(\frac{\theta_f}{2}\right) \right) \qquad (14)$$

$$\sin\left(\frac{\theta_f}{2}\right) \approx 1.22\frac{\lambda}{D} = 1.22\frac{c}{fD} \qquad \lambda \ll D \text{ (for circular transducer)} \qquad (15)$$

As described in Section 2.2, two beam spread attenuation terms appear in this experiment: $\alpha_{S_{in}}(f, d_1)$ and $\alpha_{S_{out}}(f, d_2)$. The first corresponds to the spread of the ultrasonic beam when the SensComp transducer acts as an emitter and the mortar acts as a receiver (transmission stage), while the second corresponds to when the mortar acts as an emitter and the SensComp transducer acts as a receiver (Fig. 2). The SensComp transducer has a circular aperture size of 38.4 mm and the mortar face that acts as emitter in the second stage has a rectangular size of 40 mm. Their pattern diagrams were measured to assess the differences between the SensComp transducer and the "mortar" transducer. For this purpose, the angle of the receiver transducer with respect to the emitter was swept from 0° to 360° in 0.4° steps (900 measurements) and the distance between them was fixed to 16 cm. Fig. 5 represents the normalized energy pattern diagram from $-90°$ to 90° for both cases. As can be appreciated, both patterns are very similar and the error is less than -12 dB. Therefore, it may be considered that both emitters have similar behaviour and they have similar beam spread attenuation. Consequently, it is assumed that $\alpha_{S_{in}}(f, d_1) = \alpha_{S_{out}}(f, d_2)$.

From Eq. (14), $d_{cal} = d_1 + d_2$ and $d_1 = d_2 = 16$ cm, we can re-write $\alpha_{S,cal}(f, d_{cal})$ as Eq. (16), which shows the relationship between $\alpha_{S,cal}(f, d_{cal})$, $\alpha_{S_{in}}(f, d_1)$ and $\alpha_{S_{out}}(f, d_2)$. Then, 6 dB must be subtracted from Eq. (13) to compensate for the difference between $\alpha_{S,cal}(f, d_{cal})$ and $\alpha_{S_{in}}(f, d_1)$. We add an additional and theoretical
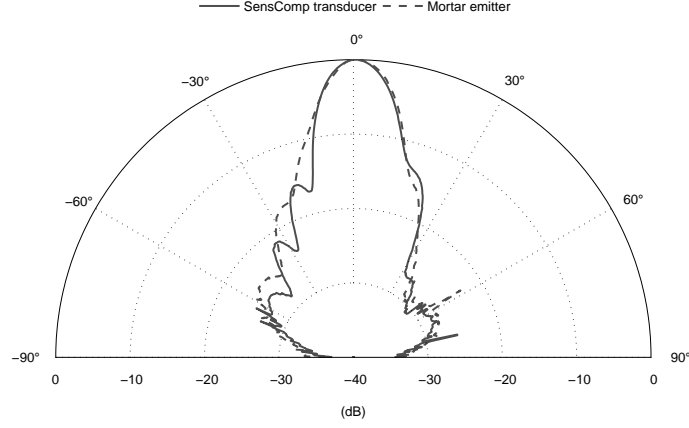
Figure 5: Energy normalized pattern diagram for SensComp transducer and Mortar

term, $\alpha_{S_{in}}(f, d_1)$, which was obtained from Eq. (14), where D and d have been fixed to 38.4 mm and 16 cm, respectively. Finally, an updated term for the calibration expression is shown in Eq. (17).

$$
\begin{aligned}
\alpha_S(f, d_{cal}) &= 20 \log 10 \left(\frac{2d_{cal}}{D} \tan\left(\frac{\theta_f}{2}\right) \right) = 20 \log_{10} \left(\frac{2(d_1 + d_2)}{D} \tan\left(\frac{\theta_f}{2}\right) \right) \\
&= 20 \log_{10} \left(\frac{2(2d_{1,2})}{D} \tan\left(\frac{\theta_f}{2}\right) \right) = 20 \log_{10} 2 + 20 \log_{10} \left(\frac{2(d_{1,2})}{D} \tan\left(\frac{\theta_f}{2}\right) \right) \\
&= 6 + \alpha_S(f, d_{1,2})
\end{aligned}
\tag{16}
$$

$$
\alpha_{cal_2}^{(NC)}(f) = \overbrace{\alpha_{equip}^{(NC)}(f)}^{\alpha_{cal_1}^{(NC)}(f) = S_{tx}(f) - S_{rx}(f)} + \alpha_{air}(f)d_{cal} + \underbrace{\alpha_S(f, d_{cal})}_{\alpha_{S_{out}}(f, d_2)} - 6 + \underbrace{20 log_{10}\left(\frac{2d_1}{D}\tan\left(\frac{\theta_f}{2}\right)\right)}_{\alpha_{S_{in}}(f, d_1)}
\tag{17}
$$

Eq. (17) includes the effects of the equipment, air gap and beam spread but it does not include the border effects, $\alpha_{B_{in}}(f)$ and $\alpha_{B_{out}}(f)$. These terms occur in the air-mortar interface (when the ultrasound beam enters the mortar) and in the mortar-air interface (when ultrasound beam exits from the mortar). In addition, they depend on the normal reflection law that establishes a transmission coefficient between two media, Eq. (18), where, I_I is the incident intensity of the ultrasound beam and I_T is the transmitted intensity, Z_1 is the acoustic impedance of medium 1 and Z_2 is the acoustic impedance of medium 2. The acoustic impedance of a medium, Z can be obtained following Eq. (19), where ρ is the density of material $[\text{kg}/\text{m}^3]$ and c is the propagation velocity $[\text{m}/\text{s}]$.

$$
T = \frac{I_T}{I_I} = \frac{4Z_1 Z_2}{(Z_1 + Z_2)^2}
\tag{18}
$$

$$
Z = \rho \cdot c
\tag{19}
$$

10

For this experiment, we have two materials, air and mortar, the data for the acoustic impedances are shown in Table 1. Taking into account Eq. (18) and the Z of both media, the transmission coefficients between air-mortar and mortar-air are the same, Eq. (20). This transmission coefficient is related to acoustic intensity and it has to be inverted (attenuation) and converted to dB to be introduced in Eq. (7) as $\alpha_{B_{in}} = \alpha_{B_{out}} = 10log_{10}\left(\frac{1}{T}\right) \approx 38$ dB. It is important to notice that this attenuation has been assumed to be not frequency dependent. This simplification is possible because the useful highest frequency for non-contact measurements (150 kHz) has a minimum wavelength of 2.2 mm and the external surface of the specimen can assumed to be smooth at this wavelength.

Table 1: Data for acoustic impedance

Material	Density ρ [kg/m^3]	Velocity c [m/s^2]	Acoustic impedance Z [kg/m/s^2]
Air (20° 70% HC)	1.18	343	405
Mortar	1427	4570	$6.5 \cdot 10^6$

$$T_{air-mortar} = T_{mortar-air} = T = \frac{4Z_{air}Z_{mortar}}{(Z_{air} + Z_{mortar})^2} = 1.5 \cdot 10^{-4} \tag{20}$$

Finally, all of the attenuation terms of Eq. (6) have been obtained and the curve $\alpha_{cal}^{(NC)}(f)$ (Eq. (21)) can be used to estimated the attenuation of material following Eq. (7). Fig. 3 represents the obtained calibration curve for non-contact measurements, which includes all the attenuation effects external to the material.

$$\alpha_{cal}^{(NC)}(f) = \overbrace{\alpha_{equip}^{(NC)}(f) + \alpha_{air}(f)(d_1 + d_2) + \alpha_{S_{cal}}(f, d_2)}^{S_{tx}(f) - S_{rx}(f)} - 6 + \alpha_{S_{in}}(f, d_1) + \alpha_{B_{in}} + \alpha_{B_{out}} \tag{21}$$

3.4. Excitation signal

To obtain the frequency dependence of the material attenuation curve, $\alpha_{mat}(f)$, the input signal should excite the desired frequency range. Different options exist to achieve this, such as narrowband signals (sinusoidal or burst signals) and broadband signals (chirp). In [17], it was demonstrated that similar accuracies are obtained with broadband signals with respect to narrowband signals but that an important improvement of time cost is reached with the first. Therefore, a chirp signal is used in this study to obtain $\hat{\alpha}_{mat}(f)$ with a single measurement. The mathematical model of a linear chirp signal is shown in Eq. (22),

$$s_{tx}(t) = A_{tx}sin\left(2\pi f_0 t + \pi\Delta_{f_{max}}t^2\right)rect\left(\frac{t - \frac{T}{2}}{T}\right) \tag{22}$$

$$\Delta_{f_{max}} = \frac{f_{max} - f_0}{T} \tag{23}$$

where A_{tx} is the amplitude of the signal, T is the active time of the signal and $\Delta_{f_{max}}$ controls the maximum frequency ($f_{max} = f_0 + T\Delta_{f_{max}}$) that is reached at T seconds (Eq. 23). To understand the importance of the

parameters, two example chirp signals and their spectra are shown in Fig. 6. It can be seen that the energy is distributed along the configured frequency bandwidth (f_0 and f_{max}) and time (T).
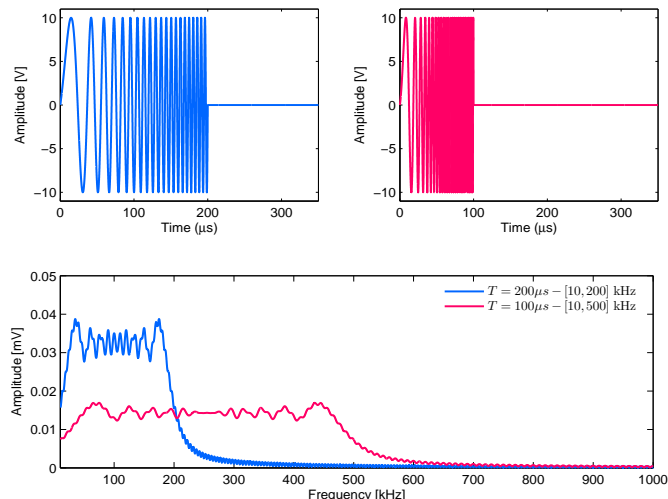

Figure 6: Two examples of chirp signals

During this work, different parameters for the transmitted signal were tested and compared ($T = [25, ..., 200] \, \mu s$ and $f_{max} = [150, ..., 1000]$ kHz), and the obtained results were consistent. Finally, the selected parameters are shown in Table 2 (the red curves shown in Fig. 6 correspond to the signal used for the contact measurements). The amplitude difference between both techniques that is due to the different amplifiers and gain factors used for each layout can be seen.

<div align="center">

Table 2: Parameters used for chirp signal for each technique

</div>

	A_{tx} [V]	f_0 [kHz]	f_{max} [kHz]	T [μs]
Contact	10	10	500	100
Non Contact	6	10	500	100

4. Results and discussion

In this section, the frequency dependent attenuation estimation of mortar using the two methods is presented, including: the non-contact method or air-coupled method and the contact method. The attenuation of the material has been evaluated from 10 kHz to 500 kHz for both methods, although the useful bandwidth has been considered between 30 kHz and 150 kHz due to the frequency response of the air-coupled transducers (see Table 2 and Fig. 3). Therefore, we will be able to compare the estimated attenuation for both methods between 30 kHz and 150 kHz.

To check the viability and robustness of both methods, three samples (A, B and C) of the material have been studied. Each sample has been measured along its main axis but from the two directions. A total of

15 measurements were taken for each sample, for each direction and for each method. Then, a total of 30 measurements for each sample and for each method were taken.

Fig. 7 shows the attenuation of material using the non-contact method, $\alpha_{mat}^{(NC)}(f)$, for the three samples. Each curve of each sample has been obtained by averaging its 30 measurements. Fig. 8 shows the average of the three curves (90 measurements) where the shadow area represents the 90 % confidence interval and the coarse line represents the averaged value. Fig. 9 and Fig. 10 represent similar data to Fig. 7 and Fig. 8 but for the contact method, $\alpha_{mat}^{(C)}(f)$.

The attenuation remains more or less constant at around 2.5 dB/cm and both methods show similar behaviour between 30 kHz and 150 kHz frequencies. Above 150 kHz, the contact attenuation has a coherent and linear growth corresponding to the dispersion zone, while non-contact attenuation does not show significant values. This happens because the system receives more noise energy during sample-measurement than during calibration-measurement out of the useful bandwidth because the sample-measurement requires higher gains. This results in a descent of the attenuation out of the useful bandwidth (above 150 kHz), as is shown in Fig. 11 and 12.

Fig. 11 and Fig. 12 compare the two methods, and the curves for non-contact and contact measurements are superimposed. Both methods show similar behaviour along the useful bandwidth and the difference between non-contact and contact measurements is less than 0.6 dB along the useful bandwidth. This error increases for frequencies higher than 150 kHz due to the worsening of the signal to noise ratio for the non-contact method. This effect can be also noticed in the standard deviation. The standard deviation for both methods is less than 5% along the useful bandwidth (30 kHz and 150 kHz), as is shown in Fig. 13. But this value increases when frequency increases (> 150 kHz), mainly for the non-contact method. In the case of the contact method, the transducers are more broadband and their useful bandwidth extends beyond 200 kHz. Therefore, this method keeps the standard deviation at around 5% for higher frequencies, as is shown in Fig. 13.
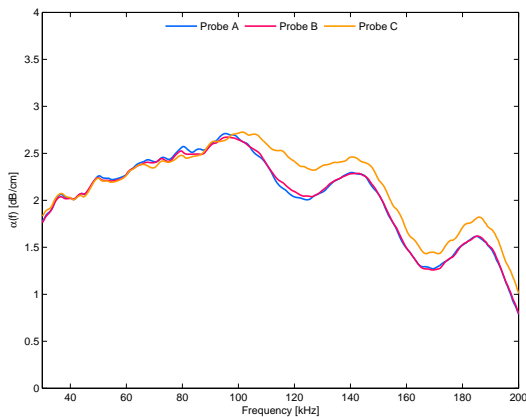

Figure 7: Material attenuation for the non-contact method ($\alpha_{mat}^{(NC)}(f)$)
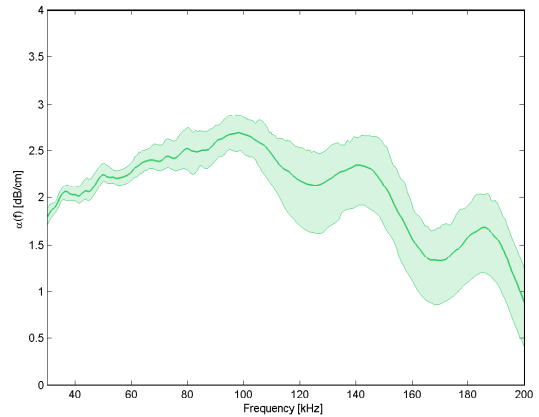

Figure 8: Average and confidence interval of material attenuation for the non-contact method ($\bar{\alpha}_{mat}^{(NC)}(f)$)
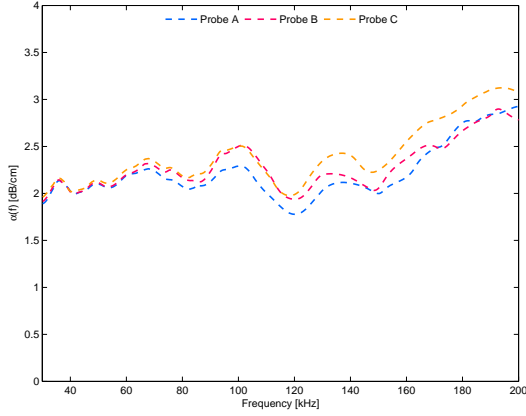
13

Figure 9: Material attenuation for the contact method $(\alpha_{mat}^{(C)}(f))$
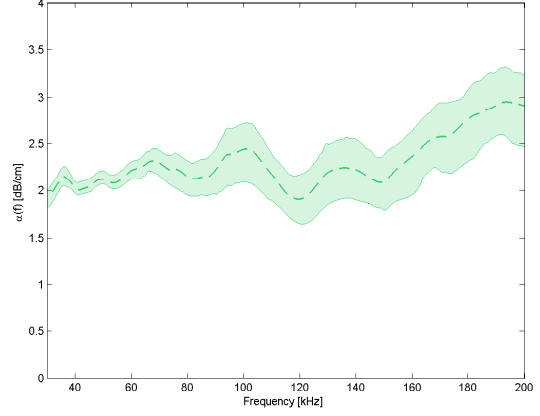

Figure 10: Average and confidence interval of material attenuation for the contact method $(\bar{\alpha}_{mat}^{(C)}(f))$
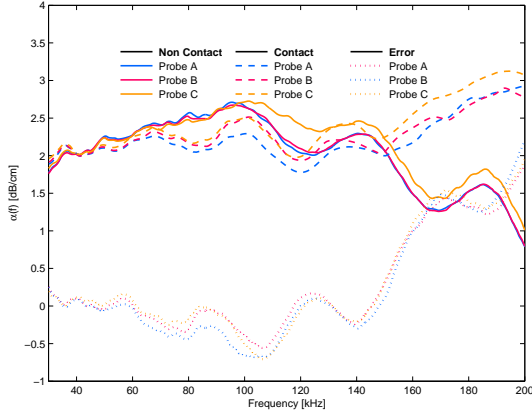

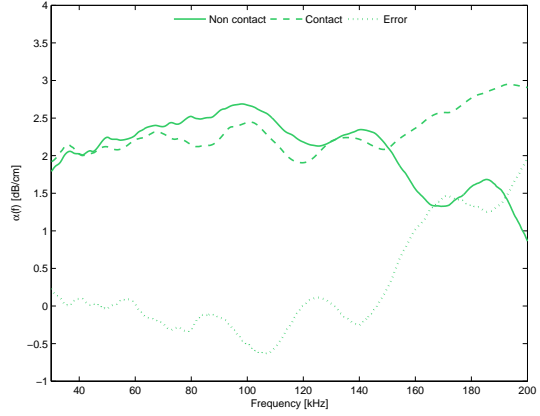**Figure 11:** Material attenuation and error curves between the non-contact and contact methods

Figure 12: Average of material attenuation and error curves between the non-contact and contact methods

5. Conclusions

In this paper, the frequency response of attenuation of cement materials has been estimated using two different ultrasonic methods: non-contact airborne ultrasound and contact ultrasound. For both cases, a through-transmission setup has been used with a broadband signal.

For the experiment, three samples of the same material were evaluated. The excitation signal was a chirp signal from 10 kHz to 500 kHz, and 30 measurements were taken for each sample and for each method. This produced 90 measurements for each method. Although the transmitted signal was a broadband signal from 10 kHz to 500 kHz, the useful bandwidth was established between 30 kHz and 150 kHz. This useful bandwidth was mainly conditioned by the non-contact transducers that were centred at 50 kHz and were able to detect useful signals from 30 kHz up to 150 kHz. Out of this band, the low signal to noise ratio of the non-contact signal did
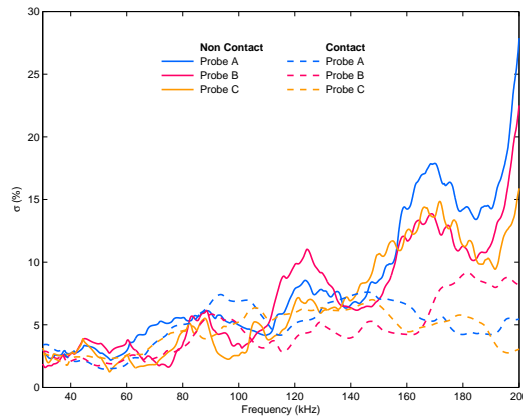
Figure 13: Standard deviation for the non-contact and contact methods

not allow us to obtain confident results. Meanwhile, the contact transducers were broadband transducers and they were able to detect signals from 10 kHz up to 1000 kHz.

Within the useful bandwidth, the difference between the non-contact and the contact measurements was less than 0.5 dB for all the frequencies. The standard deviation was also less than 5%. We conclude that both methods offer similar and confident results but the non-contact procedure does not require any kind of coupling between the transducers and the inspected material. This suggests some advantage and it avoids some measurement mistakes, such as coupling absorption or signal variation due to pressure variation between the transducers and the material. In addition, the use of a non-contact method facilitates the automation of the inspection processes.

Both methods require a calibration process to compensate for the frequency response of the equipment (cables, amplifiers, transducers and interfaces). Meanwhile, the non-contact procedure requires additional calibration and theoretical development to estimate the acoustic impedance of the inspected material to compensate for the losses that occur at the boundaries of the inspected material, and also to estimate the attenuation of the ultrasonic beam spread.

Aknowledgements

References

[1] P. Aïtcin, Binders for Durable and Sustainable Concrete, Modern Concrete Technology, Taylor & Francis, ISBN 9780415385886, 2007.
[2] N. C. V.M. Maholtra, Non destructive testing on concrete, CMC, 2003.
[3] X. G. Tang, Y. J. Xie, G. C. Long, Application of Non-Destructive Technology in Evaluating Concrete to Sulfate Attack, Advanced Materials Research 168-170 (2010) 2565–2570.
[4] K. J. Leśnicki, J.-Y. Kim, K. E. Kurtis, L. J. Jacobs, Characterization of ASR damage in concrete using nonlinear impact resonance acoustic spectroscopy technique, NDT & E International 44 (8) (2011) 721–727.

[5] C. Payan, V. Garnier, J. Moysan, P. a. Johnson, Applying nonlinear resonant ultrasound spectroscopy to improving thermal damage assessment in concrete, The Journal of the Acoustical Society of America 121 (4) (2007) EL125.

[6] M. Molero, I. Segura, S. Aparicio, M. G. Hernández, M. a. G. Izquierdo, On the measurement of frequency-dependent ultrasonic attenuation in strongly heterogeneous materials., Ultrasonics 50 (8) (2010) 824–8.

[7] M. Diallo, M. Prasad, E. Appel, Comparison between experimental results and theoretical predictions for P-wave velocity and attenuation at ultrasonic frequency, Wave Motion 37 (1) (2003) 1–16.

[8] D. Aggelis, T. Philippidis, Ultrasonic wave dispersion and attenuation in fresh mortar, NDT & E International 37 (8) (2004) 617–631.

[9] V. Garnier, B. Piwakowski, O. Abraham, G. Villain, C. Payan, J. F. Chaix, Acoustic techniques for concrete evaluation: Improvements, comparisons and consistency, Construction and Building Materials 43 (2013) 598–613.

[10] T. P. Philippidis, D. G. Aggelis, Experimental study of wave dispersion and attenuation in concrete., Ultrasonics 43 (7) (2005) 584–95.

[11] T. Seldis, Enhanced experimental approach to measure the absolute ultrasonic wave attenuation., Ultrasonics 50 (1) (2010) 9–12.

[12] P. Gaydecki, F. Burdekin, The propagation and attenuation of medium-frequency ultrasonic waves in concrete: a signal analytical approach, Measurement Science ... 126.

[13] A. Shah, Y. Ribakov, C. Zhang, Efficiency and sensitivity of linear and non-linear ultrasonics to identifying micro and macro-scale defects in concrete, Materials & Design 50 (2013) 905–916.

[14] B.-C. Kim, J.-Y. Kim, Characterization of ultrasonic properties of concrete, Mechanics Research Communications 36 (2) (2009) 207–214.

[15] W. Punurai, J. Jarzynski, J. Qu, K. E. Kurtis, L. J. Jacobs, Characterization of entrained air voids in cement paste with scattered ultrasound, NDT & E International 39 (6) (2006) 514–524.

[16] W. Punurai, J. Jarzynski, J. Qu, J.-Y. Kim, L. J. Jacobs, K. E. Kurtis, Characterization of multi-scale porosity in cement paste by advanced ultrasonic techniques, Cement and Concrete Research 37 (1) (2007) 38–46.

[17] V. Genovés, J. Gosálbez, A. Carrión, R. Miralles, J. Payá, Optimized ultrasonic attenuation measures for non-homogeneous materials, Ultrasonics 65 (2016) 345 – 352.

[18] D. E. Chimenti, Review of air-coupled ultrasonic materials characterization, Ultrasonics 54 (7) (2014) 1804–1816, ISSN 0041624X.

[19] M. Kaczmarek, B. Piwakowski, R. Drelich, Noncontact Ultrasonic Nondestructive Techniques: State of the Art and Their Use in Civil Engineering, Journal of Infrastructure Systems 23 (1), ISSN 1076-0342.

[20] J. Berriman, P. Purnell, D. A. Hutchins, A. Neild, Humidity and aggregate content correction factors for air-coupled ultrasonic evaluation of concrete, Ultrasonics 43 (4) (2005) 211–217.

[21] K. Hall, Air-coupled ultrasonic tomographic imaging of concrete elements, Ph.D. thesis, University of Illinois, 2011.

[22] V. Genovés, J. Gosálbez, R. Miralles, M. Bonilla, J. Payá, Ultrasonic characterization of {GRC} with high percentage of fly ash substitution, Ultrasonics 60 (2015) 88 – 95, ISSN 0041-624X.

[23] W. Jiang, W. M. D. Wright, Multi-channel ultrasonic data communications in air using range-dependent modulation schemes, IEEE Transactions on Ultrasonics, Ferroelectrics, and Frequency Control 63 (1) (2016) 147–155, ISSN 0885-3010.

[24] W. Mason, R. Thurston, Physical Acoustics: Principles and Methods, no. v. 17 in Physical Acoustics, Academic Press, ISBN 9780124779174, 1984.

[25] T. Gomez, F. Montero, Bridging the gap of impedance mismatch between air and solid materials, in: 2000 IEEE Ultrasonics Symposium. Proceedings. An International Symposium (Cat. No.00CH37121), vol. 2, ISBN 0-7803-6365-5, ISSN 10510117, 1069–1072, 2000.

[26] UNE, EN 196-1:2005. Métodos de ensayo de cementos. Parte 1: Determinación de resistencias mecánicas, 2005.